

Electron Impact Excitation of Helium-like Oxygen up to $n=4$ levels including radiation damping

Franck Delahaye and Anil K. Pradhan

Department of Astronomy, Ohio State University
Columbus, Ohio, USA, 43210

Abstract.

The primary X-ray diagnostic lines in He-like ions are mainly excited by electron impact from the ground level to the $n = 2$ levels, but at high temperatures $n > 2$ levels are also excited. In order to describe the atomic processes more completely collision strengths are computed for O VII including for the first time all of the following: (i) relativistic fine structure, (ii) levels up to the $n = 4$, and (iii) radiation damping of autoionizing resonances. The calculations are carried out using the Breit-Pauli R-matrix (BPRM) method with a 31-level eigenfunction expansion. Resonance structures in collision strengths are delineated in detail up to the $n = 4$ thresholds. For highly charged He-like ions radiation damping of autoionizing resonances is known to be significant. We investigate this effect in detail and find that while resonances are discernibly damped radiatively as the series limit $n \rightarrow \infty$ is approached from below, the overall effect on effective cross sections and rate coefficients is found to be very small. Collision strengths for the principal lines important in X-ray plasma diagnostics, w,x,y and z, corresponding to the 4 transitions to the ground level $1s^2 (^1S_0) \leftarrow 1s2p(^1P_1^o), 1s2p(^3P_2^o), 1s2p(^3P_1^o), 1s2s(^3S_1)$, are explicitly shown. It is found that the effective collision strength of the forbidden z-line is up to a factor of 4 higher at $T < 10^6$ K than previous values. This is likely to be of considerable importance in the diagnostics of photoionized astrophysical plasmas. Significant differences are also found with previous works for several other transitions. This work is carried out as part of the Iron Project-RmaX Network.

PACS number: 34.80.Kw

Short title: Electron Impact Excitation of Helium-like Oxygen up to $n=4$ levels including radiation damping

November 4, 2018

1. Introduction

Helium-like ions provide the most important X-ray spectral diagnostics in high temperature fusion and astrophysical plasmas. The new generation of X-Ray satellites such as the Chandra X-Ray Observatory and the X-Ray Multi-Mirror Mission-Newton provide high resolution spectra of different types of astronomical objects (e.g. Kaastra *et al.* 2000, Porquet and Dubau 2000, Porquet *et al.* 2001). The high sensitivity of these observatories and the high quality of the spectra they produce requires highly accurate atomic data for a precise interpretation. The aim of the Iron Project-R-matrix calculations for X-ray spectroscopy (IP-RmaX) is to calculate extended sets of accurate collision strengths and rate coefficients for all ions of importance in X-Ray diagnostics. Among previous works, the electron impact excitation of Helium like oxygen was previously considered by Pradhan *et al.* (1981a,b) in the distorted wave and close coupling approximations for transitions up to the $n = 2$ levels. Sampson *et al.* (1983) and Zhang and Sampson (1987) used the Coulomb-Born approximation with exchange, intermediate coupling, and some resonances effects to obtain collision strengths for Helium-like ions, with atomic number Z spanning a large range of values ($4 < Z < 74$). Kingston and Tayal (1983a,b) calculated the collision strength for two transitions, from the ground state to 2^3S_1 and to $2^3P_1^o$, using the close coupling R-matrix (RM) method, and derived the corresponding effective collision strengths. Both, the Pradhan *et al.* and Kingston and Tayal calculations were in LS coupling. The present work aims at generating a more complete dataset of high reliability for O VII, including all important effects for highly charged ions such as relativistic effects, radiation damping, and resonances in higher complexes up to $n = 4$.

The method and computations are summarized in section 2. Results for the collision strengths and important issues are discussed in section 3, and the present results for the effective (Maxwellian averaged) collision strengths are compared with previous calculations. The main conclusions are given in section 4, together with an estimate of accuracy of the results.

2. Method and Computations

The collisional calculation in the present work has been carried out using the Breit-Pauli R-matrix (BPRM) method as used in the Iron Project (IP) and utilised in a number of previous publications. The aims and methods of the IP are presented in Hummer *et al.* (1993). We briefly summarise the main features of the method and calculations.

In the coupled channel or close coupling (CC) approximation the wave function expansion, $\Psi(E)$, for a total spin and angular symmetry $SL\pi$ or $J\pi$, of the $(N+1)$

electron system is represented in terms of the target ion states as:

$$\Psi(E) = A \sum_i \chi_i \theta_i + \sum_j c_j \Phi_j, \quad (1)$$

where χ_i is the target ion wave function in a specific state $S_i L_i \pi_i$ or level $J_i \pi_i$, and θ_i is the wave function for the $(N+1)^{th}$ electron in a channel labeled as $S_i L_i (J_i) \pi_i k_i^2 \ell_i (SL\pi) [J\pi]$; k_i^2 is the incident kinetic energy. In the second sum the Φ_j 's are correlation wave functions of the $(N+1)$ electron system that (a) compensate for the orthogonality conditions between the continuum and the bound orbitals, and (b) represent additional short-range correlations that are often of crucial importance in scattering and radiative CC calculations for each symmetry. The Φ_j 's are also referred to as “bound channels”, as opposed to the continuum or “free” channels in the first sum over the target states. In the relativistic BPRM calculations the set of $SL\pi$ are recoupled in an intermediate (pair) coupling scheme to obtain $(e + \text{ion})$ states with total $J\pi$, followed by diagonalisation of the $(N+1)$ -electron Hamiltonian. Details of the diagonalization and the R-matrix method are given in many previous works (e.g. Berrington *et al.* 1995).

The target expansion for the close coupling calculations consists of 31 fine-structure levels arising from the 19 LS terms with principal quantum number $n \leq 4$. The target eigenfunctions were developed using the SUPERSTRUCTURE program (Eissner *et al.* 1974) with a version due to Nussbaumer and Storey (1978). The full expansion, together with the scaling factors in the *Thomas-Fermi* potential employed in SUPERSTRUCTURE, are given at the end of table 1.

In order to estimate the quality of the target wavefunction expansion, we compare the energy levels with those from the *National Institute for Standards and Technology* (NIST) in table 1. A better criterion for the accuracy of the wavefunctions is the accuracy of the oscillator strengths for transitions in the target ion. In table 2 we compare the gf -values with the evaluated compilation from NIST for a number of dipole transitions in O VII. For the energies the agreement with the NIST values is found to be very good, within 0.05% for all levels. The oscillator strengths agree well within 10% (however, for some of the values given by NIST, the estimated accuracy is 30%). Another accuracy criterion is the level of agreement between the oscillator strengths in the length and the velocity formulations, which we also find to be a few percent for all transitions. The Einstein A-values are also presented in table 2 to enable ready application of the present collisional data in radiative-collisional models for spectral diagnostics (e.g. Porquet and Dubau 2000, Porquet *et al.* 2001).

The 19 LS terms are recoupled in the relativistic BPRM calculations into the corresponding 31 fine structure levels up to the $n = 4$ complex using the routine RECUPD that performs intermediate coupling operations including the one-body Breit-Pauli operators (Hummer *et al.* 1993). The reconstructed target eigenfunctions and the

Table 1: Energy levels compared with observed values (in Rydbergs).

Levels		E_{calc}	E_{obs}
$1s^2$	1S_0	0.0000	0.0000
$1s2s$	3S_1	41.2438	41.2315
$1s2p$	$^3P_0^o$	41.7933	41.7872
$1s2p$	$^3P_1^o$	41.7942	41.7877
$1s2p$	$^3P_2^o$	41.7997	41.7928
$1s2s$	1S_0	41.8074	41.8124
$1s2p$	$^1P_1^o$	42.2100	42.1844
$1s3s$	3S_1	48.6577	48.6509
$1s3p$	$^3P_0^o$	48.8114	48.8044
$1s3p$	$^3P_1^o$	48.8116	48.8044
$1s3p$	$^3P_2^o$	48.8132	48.8044
$1s3s$	1S_0	48.8217	48.8112
$1s3d$	3D_1	48.8930	48.8837
$1s3d$	3D_2	48.8931	48.8842
$1s3d$	3D_3	48.8935	48.8843
$1s3d$	1D_2	48.8971	48.8937
$1s3p$	$^1P_1^o$	48.9281	48.9218
$1s4s$	3S_1	51.1813	51.1798
$1s4p$	$^3P_0^o$	51.2436	51.2360
$1s4p$	$^3P_1^o$	51.2437	51.2360
$1s4p$	$^3P_2^o$	51.2444	51.2360
$1s4s$	1S_0	51.2475	51.2410
$1s4d$	3D_1	51.2767	51.2675
$1s4d$	3D_2	51.2767	51.2600
$1s4d$	3D_3	51.2769	51.2720
$1s4f$	$^3F_2^o$	51.2786	51.2698
$1s4f$	$^3F_3^o$	51.2785	51.2698
$1s4f$	$^3F_4^o$	51.2787	51.2698
$1s4d$	1D_2	51.2790	51.2739
$1s4f$	$^1F_3^o$	51.2787	51.2755
$1s4p$	$^1P_1^o$	51.2916	51.2870

Spectroscopic configurations: $1s^2$, $1s2s$, $1s2p$ $1s3s$, $1s3p$, $1s3d$, $1s4s$, $1s4p$, $1s4d$, $1s4f$.

Correlation configurations: $2s^2$, $2p^2$, $2s2p$ $2s3s$, $2s3p$, $2s3d$, $2s4s$, $2s4p$, $2s4d$, $2s4f$.

Scaling factors: $\lambda_{1s} = 0.9932$, $\lambda_{2s} = 1.0759$, $\lambda_{2p} = 0.9217$, $\lambda_{3s} = 1.0306$,
 $\lambda_{3p} = 0.9023$, $\lambda_{3d} = 0.9547$, $\lambda_{4s} = 1.0182$, $\lambda_{4p} = 0.9038$, $\lambda_{4d} = 0.9512$, $\lambda_{4f} = 1.0200$.

Table 2: Comparison of A_{ij} and g^*f values compiled by NIST and thoses obtained with SUPERSTRUCTURE (calc).

$Conf_i - Conf_k$	$Term_i - Term_k$	E_i (Ryd)	E_k (Ryd)	A_{ki}^{NIST} (s)	A_{ki}^{cal} (s)	$g * f_{NIST}$	$g * f_{calc}$
$1s2 - 1s2p$	$^1S_0 - ^1P_1^o$	0.0000	42.1844	3.309e+12	3.403e+12	6.945e-01	7.142e-01
$1s2 - 1s3p$	$^1S_0 - ^1P_1^o$	0.0000	48.9218	9.365e+11	1.004e+12	1.462e-01	1.566e-01
$1s2s - 1s2p$	$^3S_1 - ^3P_0^o$	41.2315	41.7872	7.797e+07	8.058e+07	3.143e-02	3.249e-02
$1s2s - 1s2p$	$^3S_1 - ^3P_1^o$	41.2315	41.7877	7.820e+07	8.083e+07	9.441e-02	9.757e-02
$1s2s - 1s2p$	$^3S_1 - ^3P_2^o$	41.2315	41.7928	8.033e+07	8.309e+07	1.587e-01	1.642e-01
$1s2p - 1s3s$	$^3P_0^o - ^3S_1$	41.7872	48.6509	2.505e+09	2.237e+09	1.986e-02	1.774e-02
$1s2p - 1s3d$	$^3P_0^o - ^3D_1$	41.7872	48.8837	8.982e+10	8.927e+10	6.662e-01	6.621e-01
$1s2p - 1s3s$	$^3P_1^o - ^3S_1$	41.7877	48.6509	7.512e+09	6.739e+09	5.957e-02	5.344e-02
$1s2p - 1s3d$	$^3P_1^o - ^3D_1$	41.7877	48.8837	6.735e+10	6.699e+10	4.996e-01	4.969e-01
$1s2p - 1s3d$	$^3P_1^o - ^3D_2$	41.7877	48.8842	1.213e+11	1.205e+11	1.499e+00	1.490e+00
$1s2p - 1s3s$	$^3P_2^o - ^3S_1$	41.7928	48.6509	1.249e+10	1.131e+10	9.917e-02	8.983e-02
$1s2p - 1s3d$	$^3P_2^o - ^3D_1$	41.7928	48.8837	4.481e+09	4.466e+09	3.328e-02	3.318e-02
$1s2p - 1s3d$	$^3P_2^o - ^3D_2$	41.7928	48.8842	4.033e+10	4.012e+10	4.992e-01	4.966e-01
$1s2p - 1s3d$	$^3P_2^o - ^3D_3$	41.7928	48.8843	1.613e+11	1.608e+11	2.795e+00	2.787e+00
$1s2s - 1s2p$	$^1S_0 - ^1P_1^o$	41.8124	42.1844	2.514e+07	2.509e+07	6.786e-02	6.773e-02
$1s2s - 1s3p$	$^1S_0 - ^1P_1^o$	41.8124	48.9218	5.055e+10	5.209e+10	3.735e-01	3.849e-01
$1s2s - 1s3p$	$^1S_0 - ^1P_1^o$	41.8124	48.9218	5.055e+10	5.209e+10	3.735e-01	3.849e-01
$1s2p - 1s3s$	$^1P_1^o - ^1S_0$	42.1844	48.8112	2.008e+10	2.223e+10	5.692e-02	6.303e-02
$1s2p - 1s3d$	$^1P_1^o - ^1D_2$	42.1844	48.8937	1.523e+11	1.540e+11	2.106e+00	2.130e+00
$1s3p - 1s3d$	$^3P_0^o - ^3D_1$	48.8044	48.8837	6.114e+05	6.200e+05	3.632e-02	3.684e-02
$1s3p - 1s3d$	$^3P_1^o - ^3D_1$	48.8044	48.8837	4.585e+05	4.649e+05	2.723e-02	2.762e-02
$1s3p - 1s3d$	$^3P_1^o - ^3D_2$	48.8044	48.8842	8.426e+05	8.535e+05	8.236e-02	8.338e-02
$1s3p - 1s3d$	$^3P_2^o - ^3D_1$	48.8044	48.8837	3.057e+04	3.099e+04	1.816e-03	1.841e-03
$1s3p - 1s3d$	$^3P_2^o - ^3D_2$	48.8044	48.8842	2.809e+05	2.841e+05	2.746e-02	2.775e-02
$1s3p - 1s3d$	$^3P_2^o - ^3D_3$	48.8044	48.8843	1.127e+06	1.143e+06	1.539e-01	1.560e-01
$1s3s - 1s3p$	$^1S_0 - ^1P_1^o$	48.8112	48.9218	3.864e+06	3.958e+06	1.180e-01	1.210e-01
$1s3d - 1s3p$	$^1D_2 - ^1P_1^o$	48.8937	48.9218	7.410e+04	8.082e+04	3.508e-02	3.832e-02

resulting target energies reproduce to 10^{-5} Ryd the results from SUPERSTRUCTURE, verifying that the algebraic operations have been carried out self-consistently and without loss of accuracy. The collision strengths have been calculated for electron energies $0 \leq E \leq 200$ Ryd. This wide energy range ensures a good coverage of the region where resonances up to the $n = 4$ complex are important, as well as the higher energy region where no resonance have been included (all channels are open) but where the background collision strengths still make a significant contribution to the Maxwellian averaged rate coefficient for electron temperatures of interest.

The inner region R-matrix basis set included 50 orbitals per angular momentum. Because of the importance of the near threshold resonances in the Maxwellian average rate coefficient, careful attention has been devoted to the resolution and a precise mesh has been chosen. A mesh of 10^{-4} Ryd was selected for the region where resonances are important, and a coarser mesh for the region where all channel are open. We included the contribution to the collision strengths from all symmetries with total angular momentum J and both odd and even parities, $J\pi \leq (\frac{35}{2})^{o,e}$. The contribution of higher partial waves was included using the Coulomb-Bethe approximation via the ‘top-up’ facility in the asymptotic region program STGF of the R-matrix package (Burke and Seaton 1986; modified by W. Eissner and G.X. Chen).

3. Results and discussion

In figures 1 and 2 we present the collision strengths for transitions from the ground state to levels in the $n = 2$ complex, and to levels in the complex $n = 3$ respectively. The high resolution of the calculations with a large number of points allow us to resolve clearly all the resonances up to the last threshold in the $n=4$ complex. We delineate the Rydberg series converging to the different series limits in all three complexes. In both figure 1 and figure 2, the identification of the Rydberg series converging to $n=3$ and $n = 4$ thresholds has been marked. The doubly excited ($e + O VII$) $\rightarrow O VI$ resonance complexes, KMM, KMN etc.. converging towards the different $n = 3$ and $n = 4$ levels are clearly resolved. We can anticipate from figure 2 that, for some transitions, the low magnitude of the background and the high density of the resonances will make the contribution of these resonances converging to the $n = 4$ complex very important and dominant. This is confirmed by our work (discussed later).

3.1. Radiation Damping

It has been previously shown (Presnyakov and Urnov 1979, Pradhan 1981, Pradhan and Seaton 1985), that radiation damping may have significant effect on the resonances in collision strengths for highly charged ions since the radiative decay rates may be large and may compete with autoionization rates, i.e. the effect of dielectronic recombination

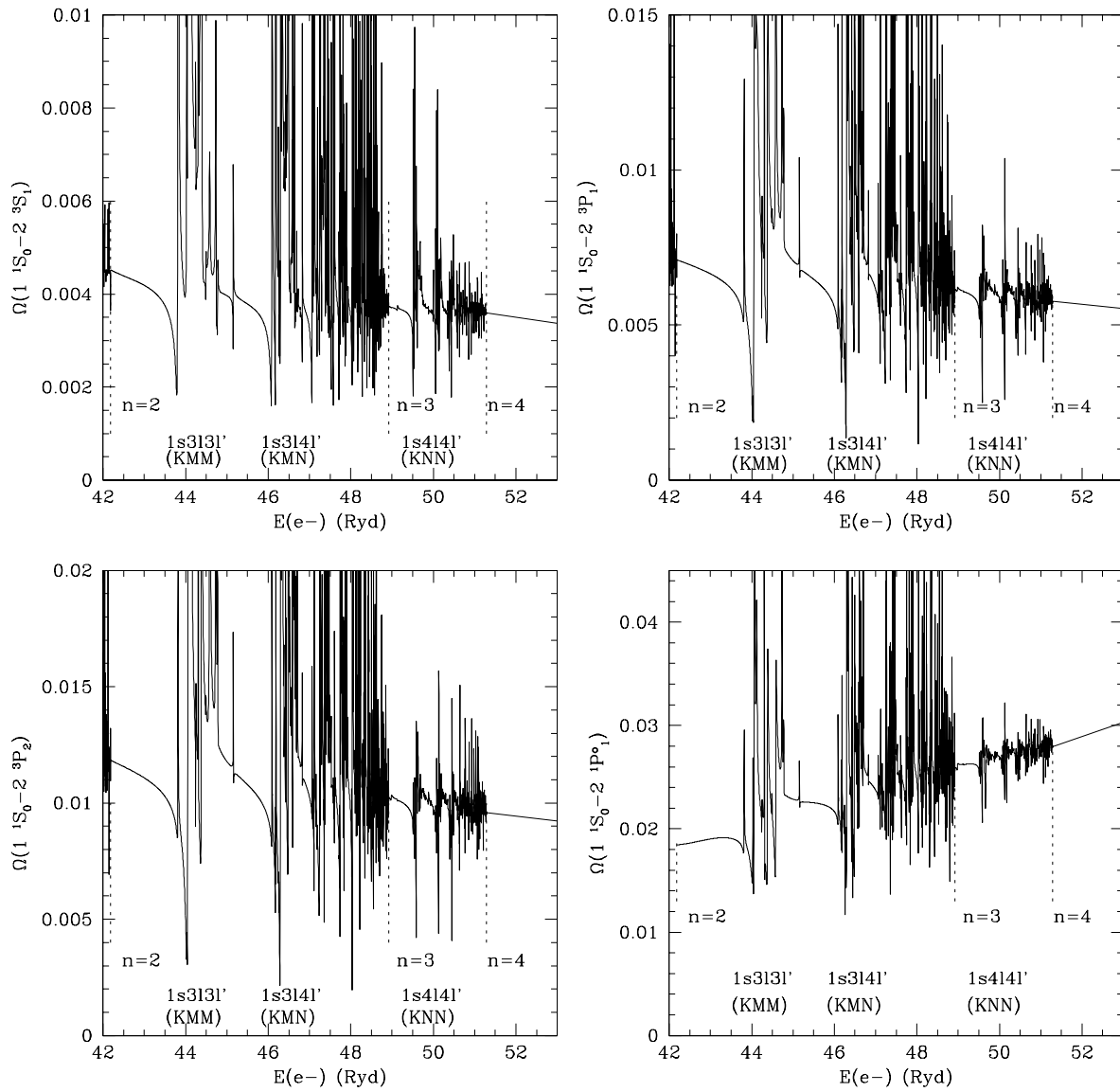


Figure 1. Collision strengths for transition for the principal lines, z, x, y and w (from ground state $1s^2 \ ^1S_0$ to 2^3S_1 , $2^3P_1^o$, $2^3P_2^o$, $2^1P_1^o$).

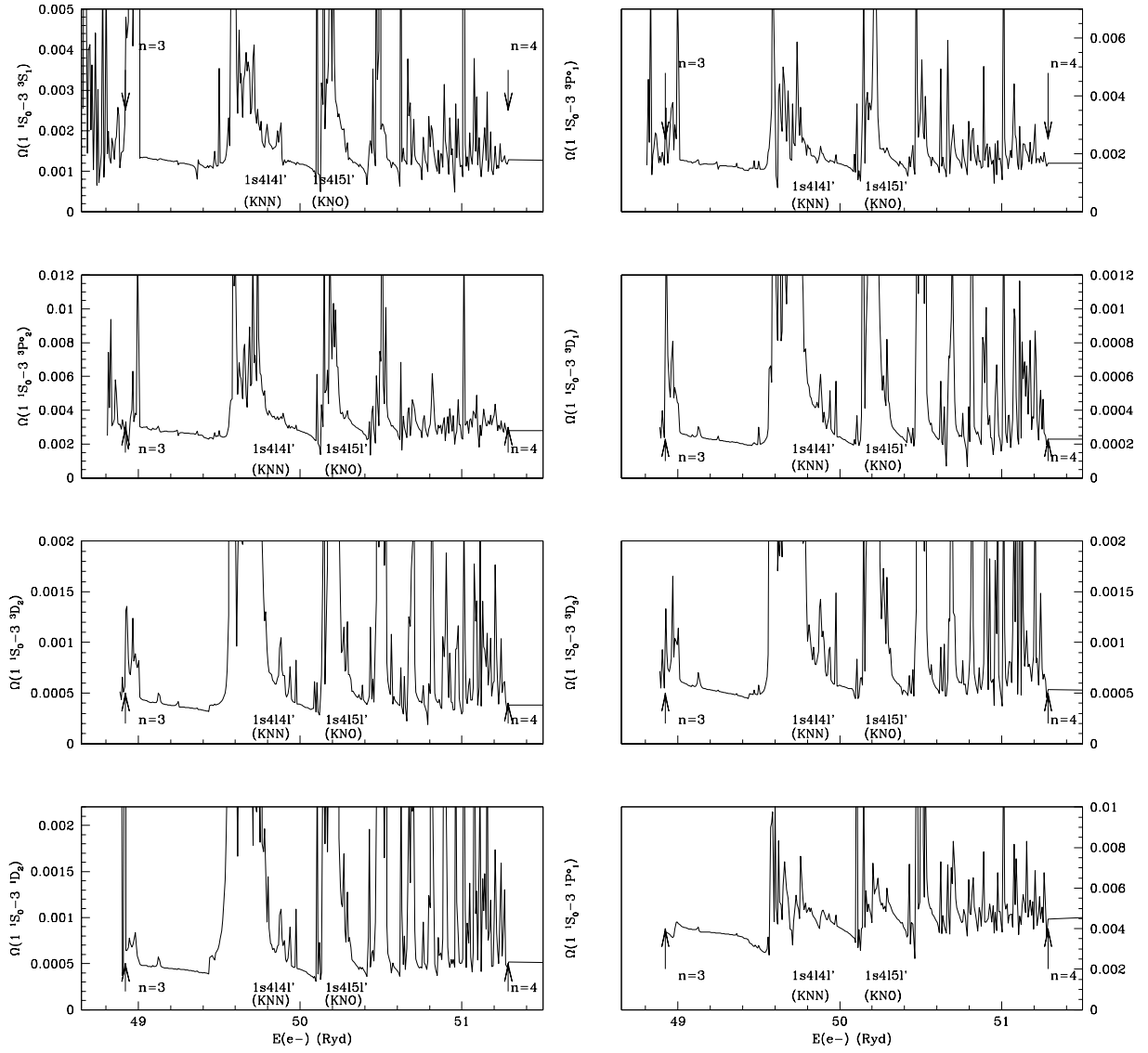


Figure 2. Collision strength for transition from the ground state to the complex with principal quantum number $n=3$. $1s^2 \ ^1S_0 \rightarrow 3^3S_1, 3^3P_1^o, 3^3P_2^o, 3^3D_1, 3^3D_2, 3^3D_3, 3^1D_2, 3^1P_1^o$

on electron impact excitation. We studied in detail the radiation damping effect of dielectronic recombination, on resonance structures, collision strengths, and rate coefficients. In figures 3 and 4, we present the Rydberg series converging to the $n = 2$ and $n = 3$ levels coupled to the ground state 1^1S_0 via strong dipole transitions, $2^1P_1^o$ (figure3) and $3^1P_1^o$ (figure4). Since the autoionization rates decrease as n^{-3} , and the radiative rate remains constant, radiation damping increases with n and the resonances are wiped out as the series limit is reached. We illustrate the effect for one total (e + ion) symmetry $J\pi = 1^e$. It can be seen how effective the diminishing of resonances is as we approach the threshold. The overall effect of damping, on the averaged collision strength, can be up to a factor two (figure5). However, the region where the effect is important is very small, just below the threshold of convergence. It is called the 'quantum defect region', since we use the Bell and Seaton (1985) (see also Pradhan and Seaton 1985) multi-channel quantum defect theory in this region. In figures 4 and 5 this region corresponds to $\Delta E = 0.36$ Ryd ($\nu_{min} = 10$). Overall however we find that for O VII the effective collision strengths and the rate coefficients are not significantly affected (figure 6 and 7). Indeed, in figure 6, damped and undamped effective collision strength Υ curves are indistinguishable (solid line).

Figures 4 and 5 show that below threshold the collision strength is constant. This is due to the high value of the effective quantum number reached in our calculations ($\nu \approx 100$), sufficient to illustrate graphically the effect of radiation damping up to the region where the resonances are almost completely damped. In order to resolve all resonances converging to the different thresholds of interest, we used an ν -mesh with about 1000 points for each interval ($\nu, \nu + 1$). In the quantum defect region the Coulomb potential dominates the scattering process. In order to directly demonstrate the effect of radiation damping in figures 4 and 5, we show that the collision strengths converge toward the background value calculated neglecting the long-range non-dipole potentials. However, just above the threshold the potential is not only Coulombic but multipole contributions are also important. In order to isolate the effect we switched-off the multipole contributions so that there is continuity across the threshold and only the radiation damping effect is illustrated.

3.2. *Effective Collision Strengths*

The Maxwellian averaged collision strengths

$$\Upsilon(T) = \int_0^\infty \Omega_{ij}(\epsilon_j) e^{-\epsilon_j/kT} d(\epsilon_j/kT), \quad (2)$$

have been computed for all transitions among levels up to the $n = 4$. As has been shown for He-like Fe XXV (Kimura et al 1999, 2000, and Machado-Pelaez et. al. 2001), the resonances arising from the complex $n = N + 1$ have a strong effect on transitions to

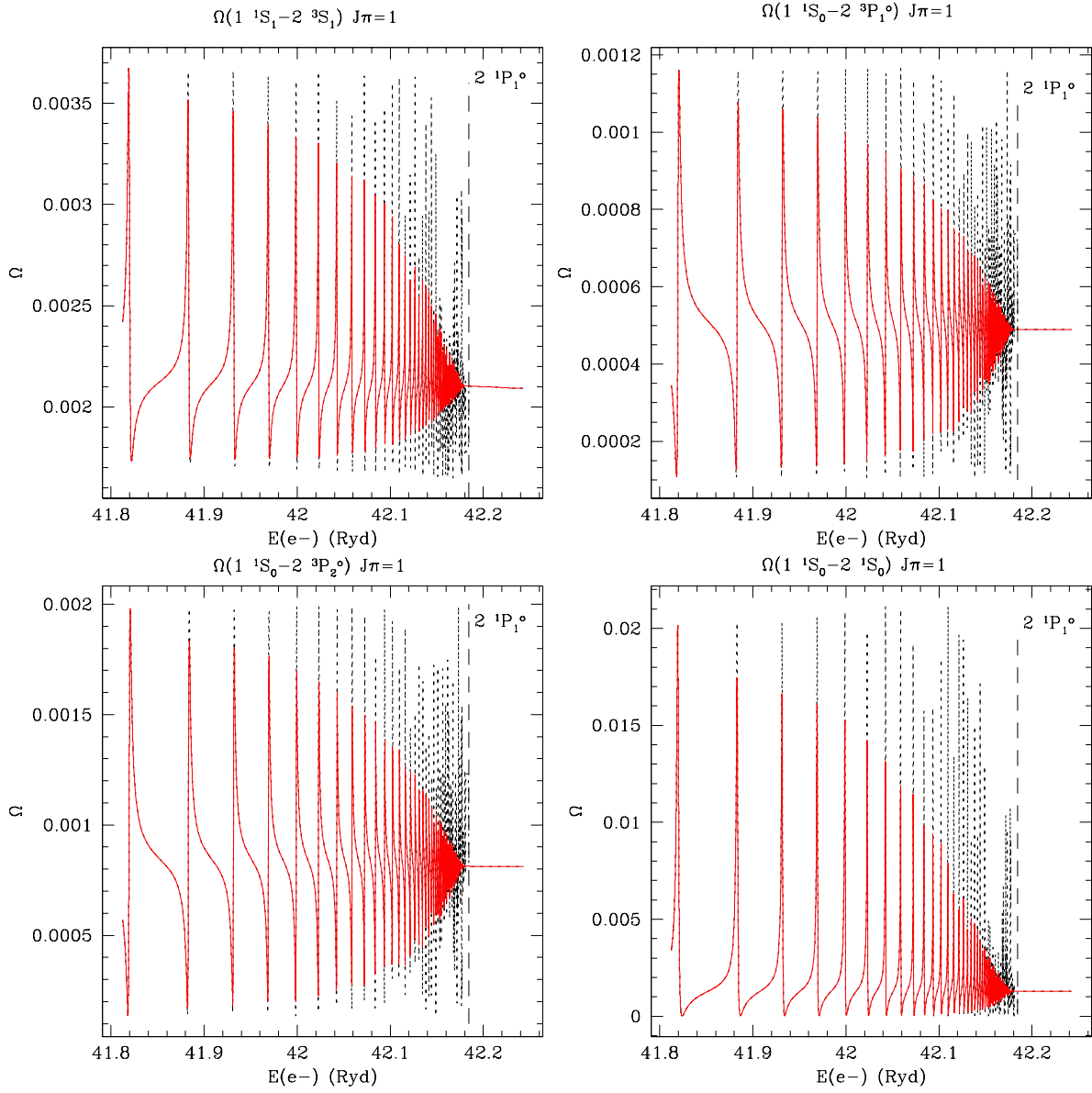


Figure 3. Partial Collision strength for transition from ground state $1s^2 \ ^1S_0$ to 2^3S_1 , $2^3P_1^\circ$, $2^3P_2^\circ$, 2^1S_0 . dashe line: resonance for $J\pi = 1_{even}$ converging to $2^1P_1^\circ$; solid line: resonance for $J\pi = 1_{even}$ converging to $2^1P_1^\circ$ damped by recombination.

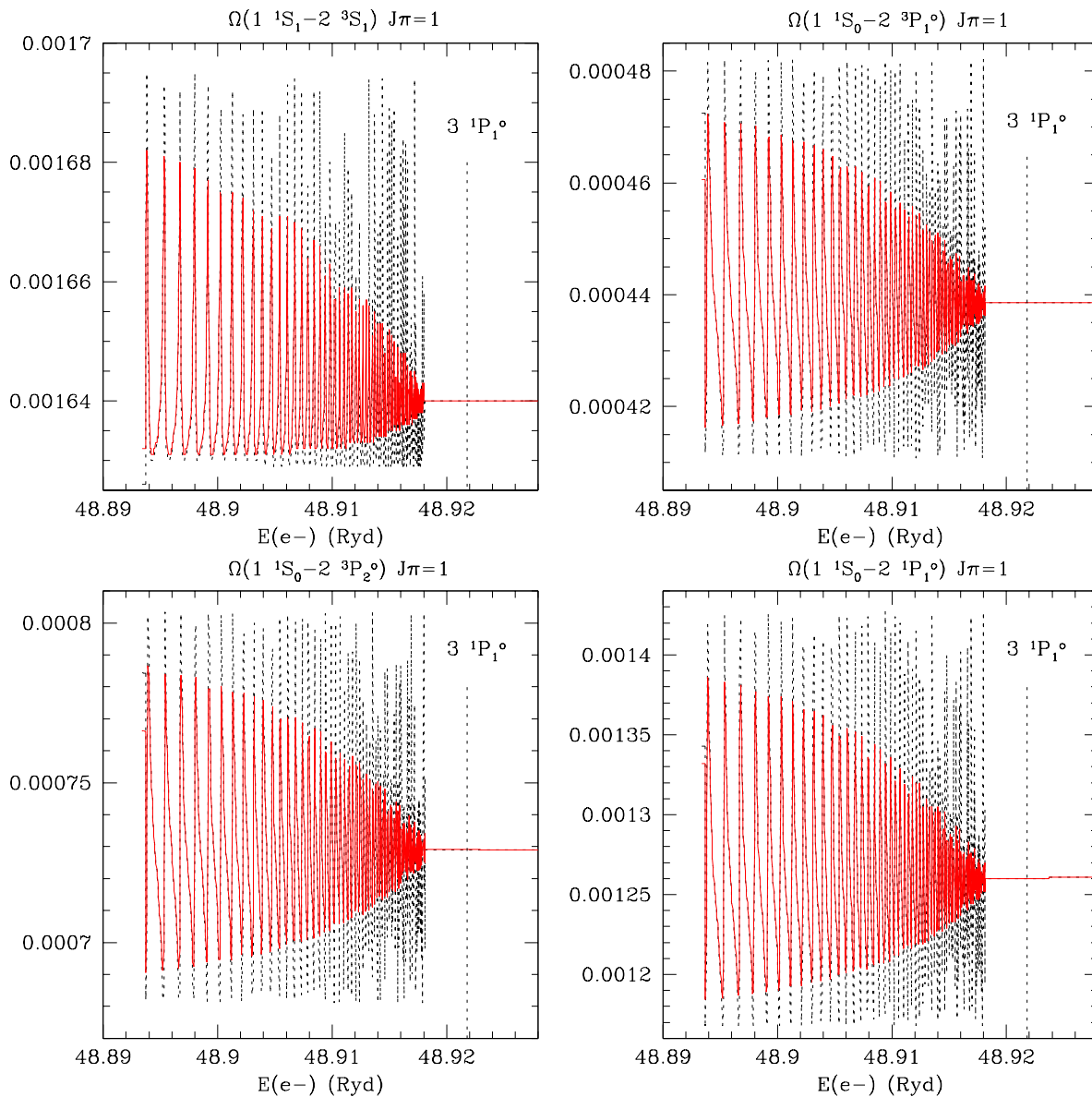


Figure 4. Partial Collision strength for transition from ground state $1s^{21}S_0$ to 3^3S_1 , $3^3P_1^o$, $3^3P_2^o$, $3^1P_1^o$ dashe line: resonance for $J\pi = 1_{even}$ converging to $3^1P_1^o$; solid line: resonance for $J\pi = 1_{even}$ converging to $3^1P_1^o$ damped by recombination.

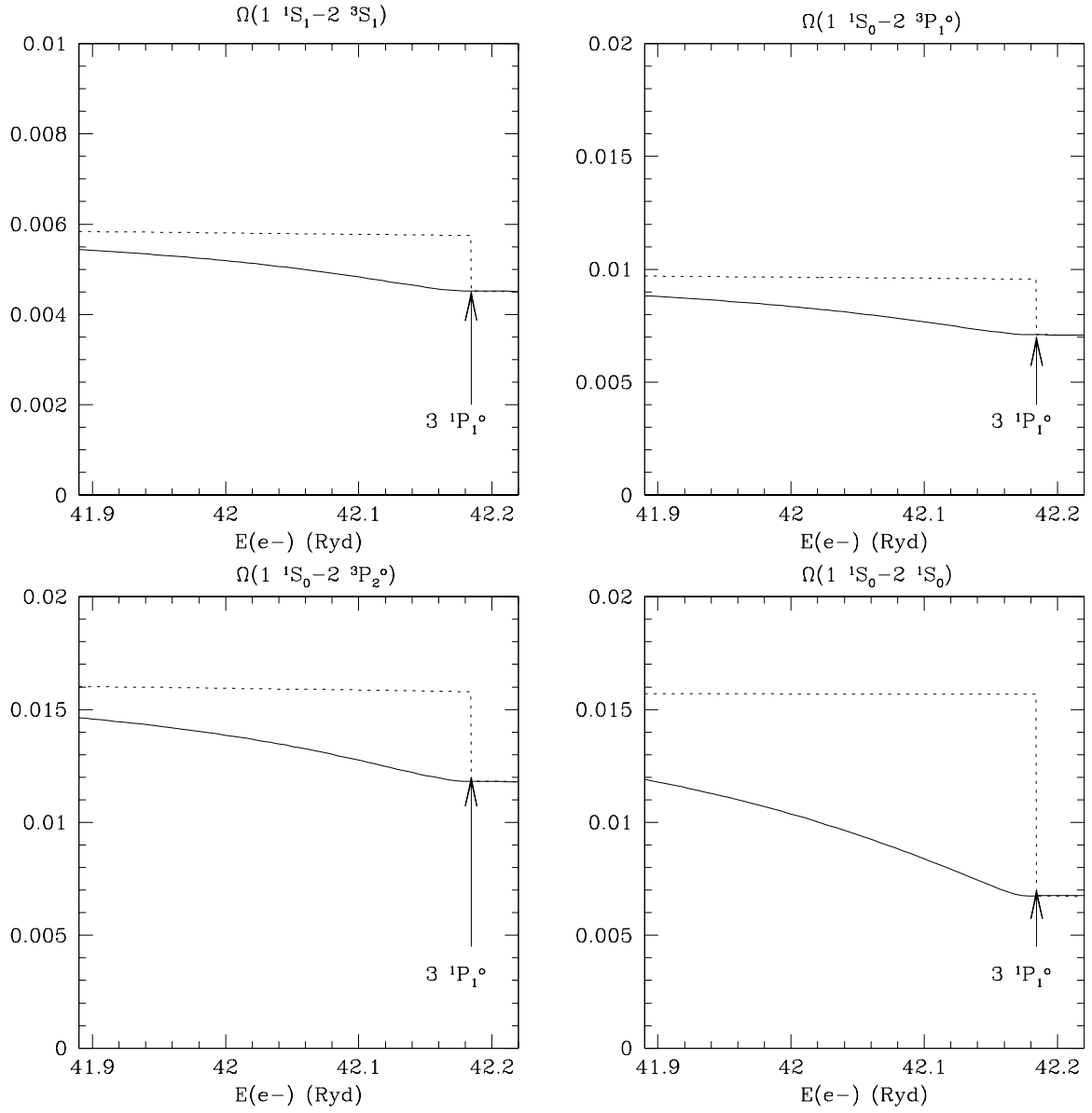


Figure 5. Total averaged Collision strength for transition from ground state $1s^{2^1}S_0$ to 2^3S_1 , $2^3P_1^o$, $2^3P_2^o$, 2^1S_0 between 2^1S_0 and $2^1P_1^o$ thresholds. dashed line: No damping; solid line: Damping effect

the complex $n = N$. Along with the full calculation including all the 31 fine structure states up to $n = 4$, we considered a smaller target model, including all 17 levels up to $n = 3$ to compare the effect of the resonances. figures 6, 7 and 8 show the effective collision strengths for transitions from the ground state to the $n = 2$ levels, as well as transitions among levels of the $n = 2$ complex, and transitions from the ground to levels of the $n = 3$ complex. We find that for some transitions the contribution from the higher $n = 4$ resonances gives rise to a factor of two increase in the effective collision strengths at the temperature of maximum abundance of O VII ($T \approx 2 \times 10^6$).

We compared the effective collision strengths with previous calculations for the principal lines w, x, y, z, (figure 6a 6b and 6d) corresponding to the 4 transitions to the ground level $1s^2 ({}^1S_0) \leftarrow 1s2p({}^1P_1^o), 1s2p({}^3P_2^o), 1s2p({}^3P_1^o), 1s2s({}^3S_1)$ respectively, that are of primary interest in X-ray spectral diagnostics (e.g. Gabriel and Jordan 1969, Pradhan 1982, Porquet et. al. 2001). Some other transitions are also compared for which the data are available in literature. Illustrative results are presented for the four principal lines (figure 6) as well as four other transitions within the $n = 2$ complex (figure 7).

Generally the agreement between the different calculations, depending on the transition and temperature, is between 10 - 30%. However, for some transitions (including the important z-line transition) the differences are larger in some temperature ranges. Basically, these differences stem from (i) the coupling effects due to the $n = 3$ and $n = 4$ levels in the close coupling expansion, (ii) relativistic effects included through the Breit-Pauli approximation, (iii) improved delineation of resonances with high-resolution, and (iv) ensuring convergence with complete ‘top-up’ of partial waves. All of these four factors are important in determining the final effective collision strength.

In figure 6 we present the transition from the ground level to the different fine structure levels with $n = 2$. The z-line (figure 6a) presents the biggest difference with previous calculations, especially at low temperatures. There is a factor 2 difference with Pradhan *et al.* (1981, crosses), and between 30 % and a factor of 2 with Kinston and Tayal (1983, dot-dashes) for $T < 2 \cdot 10^5$ K, both lying below the present values. Above 10^5 K the difference is within 10%. The most striking difference however is with the results of Zhang and Sampson (1987, short-dashes) that are much lower and start to converge only at very high temperatures. One might ascribe it to the fact that resonances are not fully considered in their work.

The primary cause of differences with previous works is the resolution of complexes of resonances near threshold, *in between the $n = 2$ levels*, where high resolution is crucial and detailed fine structure plays an important role. The Ω_{ij} at low energies determines the effective collision strength at low temperatures since $\Upsilon_{ij}(T \rightarrow 0) = \Omega_{ij}(E \rightarrow 0)$. The importance of the resonances for this transition was already shown by Pradhan *et al.* (1981) and Kinston and Tayal (1983a,b) in their LS coupling calculations, both of

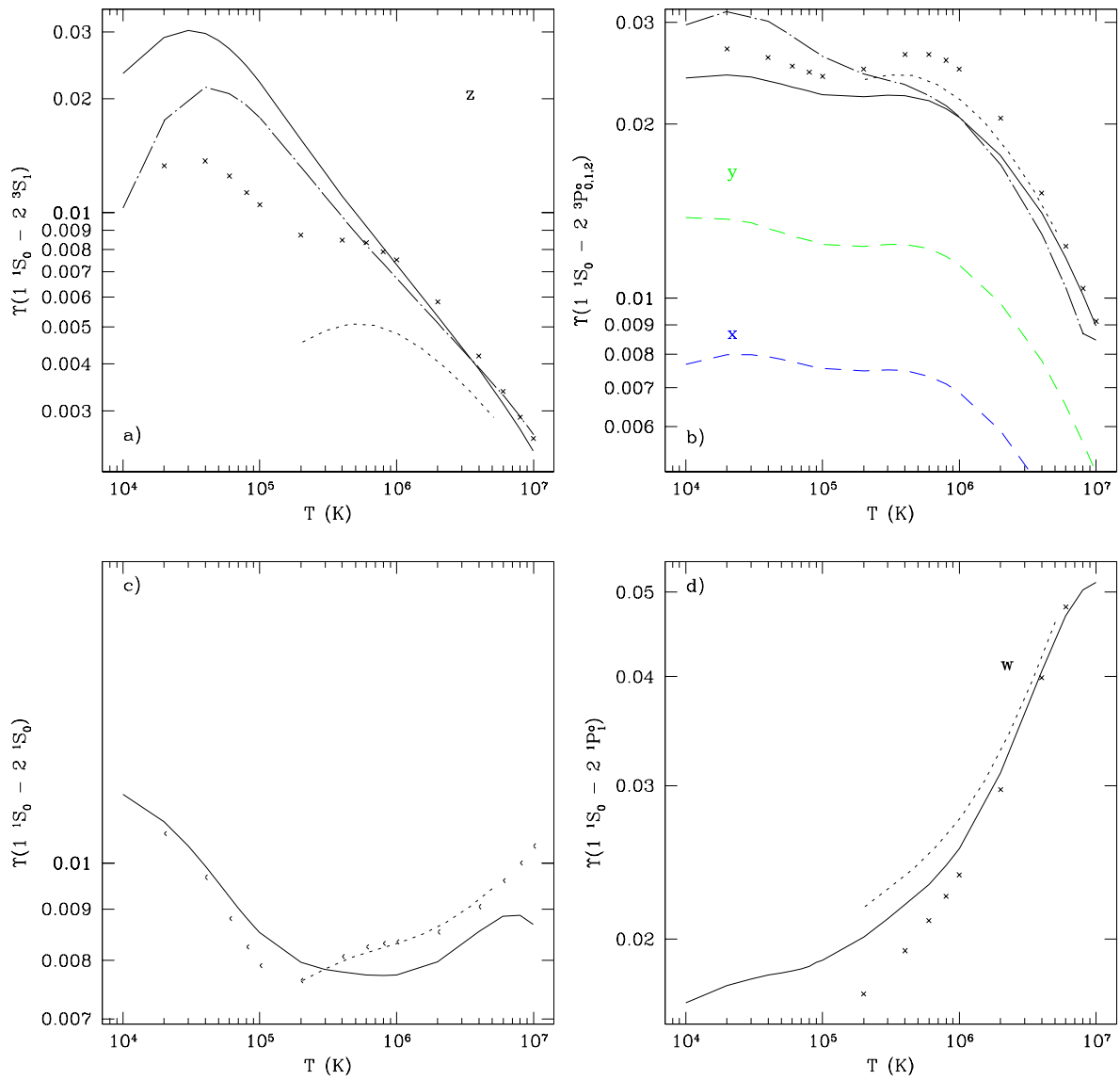


Figure 6. Effective Collision Strengths for the principal lines (z, x, y, w). solid line: Present work (long dashes on 6b: x and y; solid = $(x+y)$) dot-dashe line: Kingston and Tayal (1983) short-dashe line: Zhang and Sampson (1987) Crosses: Pradhan *et al.* (1981) Note: The two curves with and without radiation damping effect are indistinguishable (solid line).

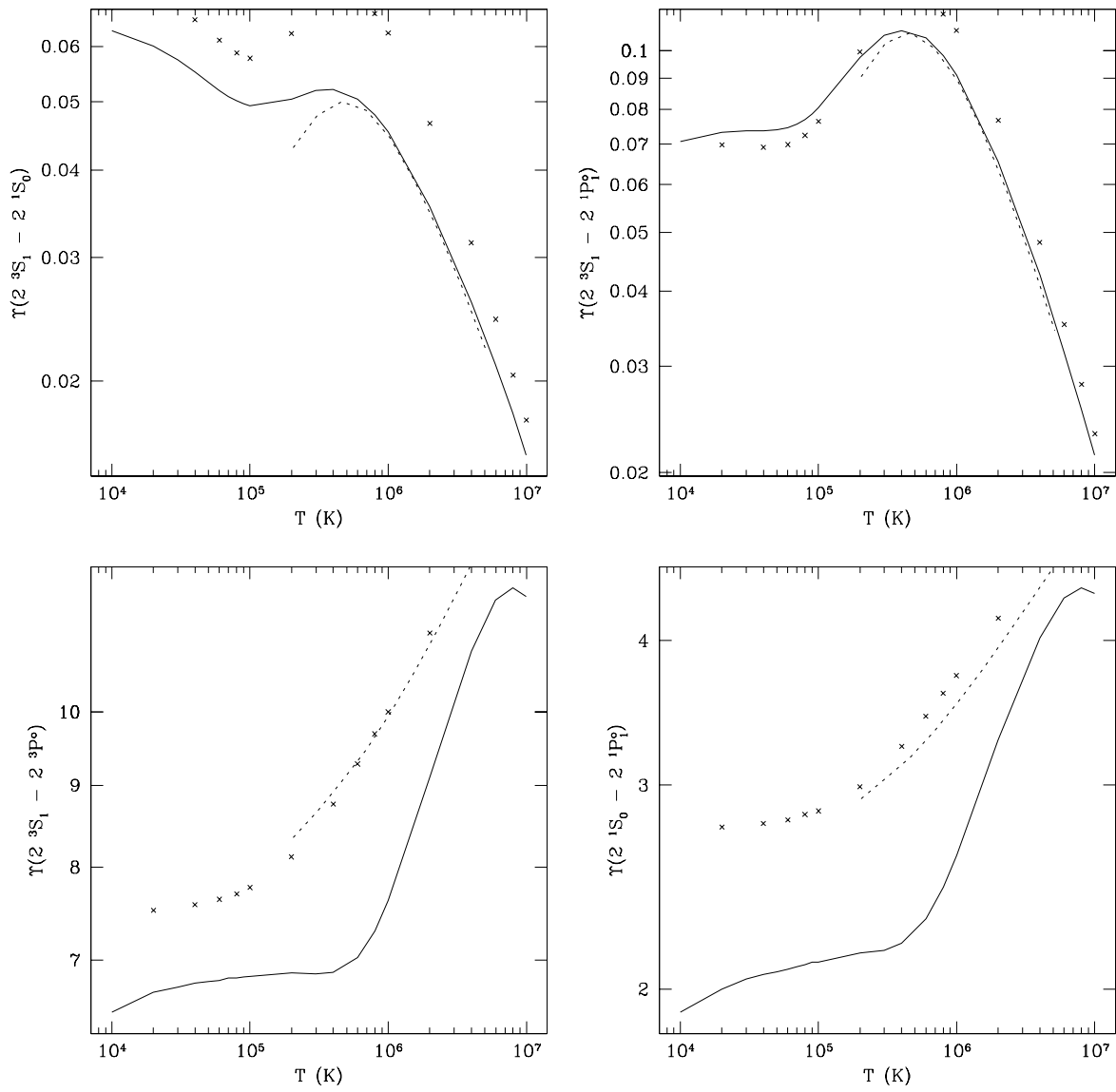


Figure 7. Effective Collision Strengths for transitions within the $n = 2$ complex. solid line: Present work dashed line: Zhang and Sampson (1987) crosses: Pradhan *et al.* (1981)

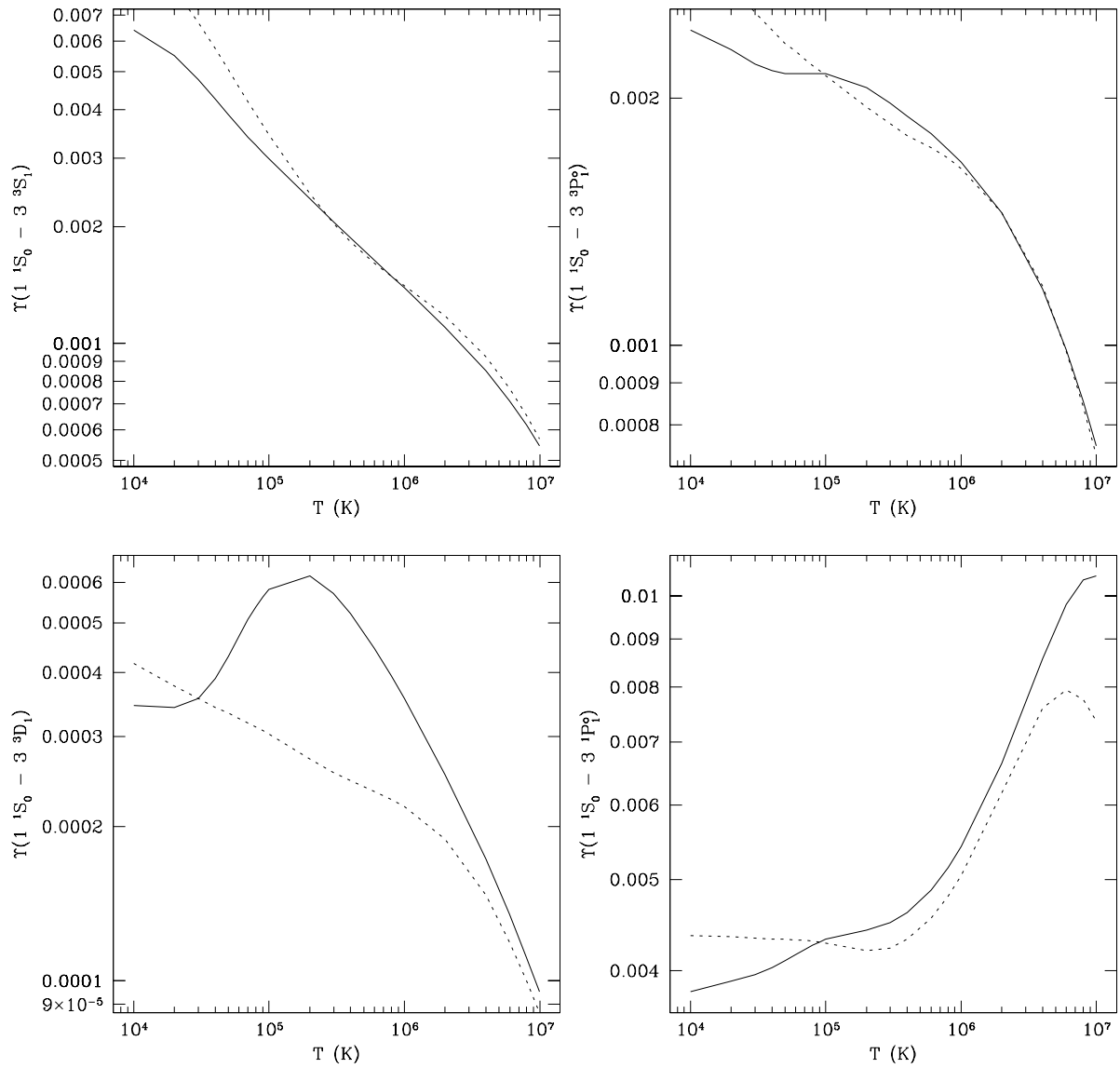


Figure 8. Effective Collision Strengths for transitions from $1s^2 \ ^1S_0$ to the $n = 3$ complex. solid line: Present work up to $n = 4$ dashed line: Present work up to $n = 3$ Note: The effect of resonance arising from $n = 4$ complex may have a major effect on transition to the $n = 3$ complex (a factor 2 for $1 \ ^1S_0 - 3^3D_1$)

whom obtain results significantly higher than Zhang and Sampson (1987). The present results demonstrate the need for a relativistic and high-resolution calculation in order to accurately obtain the excitation rates at low temperatures.

With the exception of Zhang and Sampson (1987), the previous works did not consider fine structure. Therefore the effective collision strengths for the $1^1S_0 - 2^3P_{2,1}^o$ transitions, corresponding to the forbidden and intercombination lines x and y, are shown individually in figure 6b, as well as added together $\Upsilon(x + y)$. The difference with all others is no more than 20% at all temperatures.

For the dipole allowed transition ($1^1S_0 - 2^1P^o$), corresponding to the w-line, the high temperature rates are within 10%. But still, the low temperature rates are higher by 20% than those from Pradhan et. al. (1981, crosses).

The strong dipole transitions among the excited $n = 2$ levels ($2^3S_1 - 2^3P^o$ and $2^1S_0 - 2^1P^o$) (figures 7c and 7d) are very important in spectral diagnostics calculations since they enable the collisional coupling at high electron densities that affects the x, y, and z lines. This also has implications for the competition between the effect of collisional redistribution among these lines, and photoexcitation by background ultraviolet radiation, if present in the X-ray source (e.g. Porquet *et al.* 2001). The total multiplet collision strength for this transition differs from earlier works by up to 30%.

4. Conclusion

Some of the general conclusions of the paper are as follows.

1. The most complete close coupling calculation using the Breit-Pauli R-Matrix method has been carried out for helium-like oxygen, including resonances up to $n = 4$ levels. Detailed studies of radiation damping indicate that it may have a significant effect on the detailed collision strengths in a small energy region below the threshold(s) of convergence, but not on the effective collision strengths. However, radiation damping is important for higher-Z elements since the transition probabilities increase with Z (Pradhan 1983a,b has found the effect on the z-transition to be 9% in Υ for Fe XXV at the temperature of maximum abundance of helium-like iron).

2. It is verified that the effects of coupling and resonances from the $n = N + 1$ complex play an important role in effective collision strengths for the transitions to the complex $n = N$.

3. The new results for the important z-line transition should significantly affect the analysis of O VII X-ray spectra from photoionized sources (e.g. active galactic nuclei), where O VII may be abundant at relatively low temperatures. In collisional ionized (coronal) sources the new results may not affect the theoretically computed line intensities significantly at temperatures close to maximum abundance, but should still do so at lower temperatures. It would be preferable to employ the present data in future

collisional-radiative and photoionization models.

4. As all relevant atomic effects in electron-ion collisions have been considered, and resonances have been carefully delineated, we should expect the present results to be of definitive accuracy. Nonetheless, we conservatively estimate the precision to be about 10-20%.

5. All data will be electronically available from the first author from delahaye@astronomy.ohio-state.edu.

The authors would like to thank Dr. Werner Eissner for immense help with many aspects of this work. We also thank Guo-Xin Chen for the new and efficient version of STGF including radiation damping used in these calculations. This work was supported partially by the U.S. National Science Foundation and by NASA. The computational work was carried out on the massively parallel Cray T3E and the vector processor Cray T94 at the Ohio Supercomputer Center in Columbus, Ohio.

References

- Bell R.H., Seaton M.J., 1985, *AdSpR* 15, 37
 Berrington K.A., Burke P.G., Chang J.J., *et al.*, 1974, *Comput. Phys. Commun.* 8, 149
 Berrington K.A., Burke P.G., Le Dourneuf M., *et al.*, 1978, *Comput. Phys. Commun.* 14, 367
 Berrington K.A., Eissner, W. and Norrington, P.H. 1995 *Comput. Phys. Commun.* 92 290
 Burke P.G., Seaton M.J., 1971, *Math. Comput. Phys.* 10, 1
 Burke P.G., Hibbert A., Robb W.D., 1971, *J. Phys. B* 4, 153
 Burke, V. M. and Seaton, M. J. 1986 *Journal Of Physics B* 19 L533
 Eissner W., Jones M., Nussbaumer H., 1974, *Comput. Phys. Commun.* 8,270
 Kaastra J.S., Mewe, R., Liedahl, D.A., Komosa, S., and Brinkman, A.C. 2000 *Astron. Astrophys.* 354 L83
 Kingston A.E., Tayal S.S., 1983, *J. Phys. B* 16, 3465
 Kingston A.E., Tayal S.S., 1983, *J. Phys. B* 16, L53
 Porquet D, Mewe R, Dubau J, Raassen A J J, and Kaastra J S 2001 *Astron. Astrophys.* 376 1113
 Porquet D and Dubau J 2000 *Astron. Astrophys. Suppl.* 143 495
 Pradhan A.K., 1981 *Physical Review Letters* 47 79
 Pradhan A.K., 1982 *Astrophys. J.* 263 477
 Pradhan A.K., 1983 *Physical Review A* 28 2113 (a) 2128 (b)
 Pradhan A.K., Seaton M.J., 1985, *J. Phys. B* 18, 1631
 Pradhan A.K., Norcross D.W., Hummer D.G., 1981, *Ap. J.* 246, 1031
 Pradhan A.K., Norcross D.W., Hummer D.G., 1981, *Phys. Rev. A* 23,619
 Presnyakov and Urnov A.M., 1979, *J. Phys. B* 8, 1280
 Sampson D.H., Goett S.J., Clark R.E.H., 1983, *Atomic Data Nuclear Data Tables* 29,467
 Zhang H.L., Sampson D.H., 1987, *Ap. J. Supp. Ser.* 63, 487